Bulletin of the Seismological Society of America, Vol. 106, No. 4, pp. –, August 2016, doi: 10.1785/0120150302

The 11 October 2010 Novaya Zemlya Earthquake: Implications for Velocity Models and Regional Event Location

by S. J. Gibbons, G. Antonovskaya, V. Asming, Y. V. Konechnaya, E. Kremenetskaya, T. Kværna, J. Schweitzer, and N. V. Vaganova

Abstract Characterizing the seismicity of Novaya Zemlya and the surrounding Arctic seas requires accurate event-location estimates. Low-magnitude events in this region are currently observed only by a small number of stations in the European Arctic, with a large azimuthal gap, making the accuracy of regional velocity models all the more important. Regional travel-time calibration is difficult given the scarcity of sufficiently well-constrained events. On 11 October 2010, a magnitude 4.5 event occurred close to the northern tip of Novaya Zemlya. This event is significant in that it is the first event in this region to have been recorded both on the relatively recent regional networks and arrays, and also teleseismically with good azimuthal coverage. We examine how well we can constrain the location and origin time using only teleseismic phases. Using only first teleseismic *P* arrivals, we constrain the epicenter to approximately 76.25° N and 64.75° E but with no depth resolution. Clear depth phases, notably on stations in the southern United States, indicate a depth between 9 and 15 km. This independent hypocenter and origin time estimate allow evaluation of regional phase travel-time prediction using different models. The predicted *Sn* travel time appears to cause the greatest variability in regional location estimates. The 3D Regional Seismic Travel Times models provide excellent *Pn* travel-time estimates for Barents Sea paths but may slightly overestimate *Sn* travel times from this source region. A modified regional 1D velocity model is defined, which best predicts *Pn* and *Sn* observations at multiple stations up to 15°. The significance of the regional travel-time models for estimating location is demonstrated for a low-magnitude event on or close to the northern island of Novaya Zemlya in March 2014, recorded with a satisfactory signal-to-noise ratio at only four stations.

Introduction

The Arctic archipelago of Novaya Zemlya, the Kara Sea, and the eastern Barents Sea are characterized by low seismicity, with fewer than 20 seismic events having been detected in the last 30 years using stations on mainland Europe and on Svalbard. The small-aperture SPITS and ARCES seismic arrays facilitate a seismic detection threshold of around magnitude 2 (Ringdal, 1997; Gibbons *et al.*, 2011) but, given the poor azimuthal coverage, the ability to locate low-magnitude events requires accurate travel-time predictions for regional phase arrivals. Calibrating seismic-velocity models requires reference events of which there are few, if any, with sufficiently low uncertainty in origin time and location. The era of Soviet nuclear weapons testing on Novaya Zemlya (Khalturin *et al.*, 2005) resulted in many large seismic events for which the source parameters are well known and which were recorded globally. All of these events, however, predate the installation of the highly sensitive SPITS array and most of the network of three-component stations. Data from the ARCES array, the KEV station at Kevo in Finland, and a few stations of the Norwegian National Seismic Network do exist for a few of the later nuclear tests. A teleseismically recorded event on 1 August 1986 was determined to be an earthquake because of the observation of clear depth phases (Marshall *et al.*, 1989), but this too predates the regional European Arctic seismic network.

Progress has nevertheless been made in constraining regional seismic-velocity models. Using body waves from a number of reasonably well-constrained events, with paths covering the European Arctic and Barents Sea, Kremenetskaya *et al.* (2001) developed a 1D velocity model called Barents, modified from the IASP91 model (Kennett and Engdahl, 1991) with a deeper Moho and higher velocities in the uppermost mantle. This provided a far better fit to observed seismic travel times in the region than the underlying global model and provided improved seismic location estimates for ground-truth events. The Barents model was evaluated and

modified (Hicks *et al.*, 2004; Schweitzer and Kennett, 2007) to be based on the more recent ak135 global model (Kennett *et al.*, 1995) and with two alternative 1D models—BAREY and BAREZ—differing in the *P*/*S* ratio in the upper mantle, being proposed to model optimally different paths from the Kara Sea to the Barents Sea. The problem of lacking path coverage for body waves from sufficiently well-constrained sources can be circumvented using surface waves for inverting the crustal and upper-mantle velocities. This can be performed for layered models (e.g., McCowan *et al.*, 1978) or accommodating lateral variations over extended regions (e.g., Levshin and Berteussen, 1979). In 2003, a project was started to construct a far more detailed model for the crust and upper mantle below the Barents Sea (Bungum *et al.*, 2005), using not only body-wave travel times for large seismic events but a large number of datasets such as deep seismic-reflection profiles and surface waves. Products of this collaboration were the Barents50 model (Ritzmann *et al.*, 2007) and BARMOD 3D (Levshin *et al.*, 2007). The latter was based on surface-wave tomography of an extended region surrounding the Barents Sea and indicated anomalously high *S*-wave velocities in the upper mantle below the eastern Barents Sea and Kara Sea (see also Ritzmann and Faleide, 2009).

Hauser *et al.* (2011) considered a probabilistic seismic model for the region comprising many diverse sets of geophysical data. Rather than specifying a single deterministic velocity at any given latitude, longitude, and depth, they consider probability distributions for seismic velocities over a 3D grid where the uncertainty at any given node is a function of the quality of constraints. A probabilistic 3D velocity model does not result in a single deterministic event-location estimate for a given set of phase arrivals, but rather a distribution of hypocenters and corresponding event origin times which fit the distribution of model parameters. The resulting clouds of hypocenters provide the analyst with a more realistic picture of the uncertainty than the classical error ellipses for which all uncertainty is assumed to be normally distributed. The primary disadvantage of this approach is that enormous computational resources are required to calculate the posterior probability distributions of event hypocenters. The event-location procedure described by Hauser *et al.* (2011) is not the only means of incorporating 3D structure into event-location procedures. The HYPOSAT algorithm and program (Schweitzer, 2001), for example, facilitates the use of multiple 1D velocity models for different groups of phases and, even using a single global velocity model, relatively unbiased solutions can be obtained by applying calibrated source-specific station corrections (e.g., Yang *et al.*, 2001; Murphy *et al.*, 2005).

Significant progress has been made toward fully 3D tomographic velocity models (e.g., Simmons *et al.*, 2012, 2015) which have been demonstrated to provide location estimates for seismic events with greatly reduced uncertainty and bias (Myers *et al.*, 2015). The Regional Seismic Travel Time (RSTT) software package (see Data and Resources) was designed to compute rapidly approximate travel times for crustal and upper-mantle phases, accounting for 3D structures. The techniques for calculating the RSTT, accounting for lateral variations in seismic-wave velocity, are described by Phillips *et al.* (2007). An initial tomographic study for regional travel times in Eurasia (described by Myers *et al.*, 2010) formed the basis for RSTT, although the underlying model is revised continually to incorporate the results from regional tomographic studies. At the time of writing, the most recent release of RSTT is from April 2014 although all previous releases of RSTT are still available for download (see Data and Resources). This allows for a systematic comparison between the performance of subsequent releases.

On 11 October 2010, an earthquake exceeding magnitude 4 occurred close to the northern tip of Novaya Zemlya. This was (by a good margin) the largest event on Novaya Zemlya since the cessation of Soviet nuclear testing (Gibbons *et al.*, 2011) and was well recorded at regional distances by the arrays and permanent three-component stations in northern Fennoscandia and on Spitsbergen, in addition to stations of the Arkhangelsk seismic network (Morozov and Konechnaya, 2013) and the network operated by the Kola Regional Seismological Center on the Kola Peninsula. Figure 1 displays the beams for the 11 October event recorded at the SPITS and ARCES seismic arrays together with the locations of the stations within 15° of the epicenter for which *Pn* and *Sn* arrival times could be read with satisfactory accuracy (Table 1). As is typical for the regional recordings of Novaya Zemlya events, *Pn* and *Sn* are the only visible phases; the *Lg* phases that dominate regional recordings along continental paths are blocked on Barents Sea paths (see Baumgardt, 2001).

This earthquake is significant because it was recorded at teleseismic distances with excellent azimuthal coverage. The event is listed in the Reviewed Event Bulletin (REB) of the International Data Center for the Comprehensive Nuclear-Test-Ban Treaty Organization with the coordinates 76.2640° N, 64.7619° E, and depth fixed to the surface. As is clear from Figure 1, there is a significant discrepancy between the REB solution (dominated by teleseismic *P* phases) and the NORSAR regional reviewed event location (see Data and Resources) which is constrained exclusively by *P* and *S* arrivals at regional and intermediate distances up to 25°: all to the west and southwest of the source region. The need to apply station corrections for source-to-receiver paths from the Barents Sea to stations in Fennoscandia has been documented (Yang *et al.*, 2001) and it is clear that an event-location estimate that does not take into account the 3D effects will be biased. The bias in the REB solution is likely to be considerably smaller, although it too is constrained to some degree by regional and far-regional phases recorded in Fennoscandia. The solution provided by the International Seismological Center (see Data and Resources) is also indicated in Figure 1. This solution is also dominated by teleseismic phases but with regional and far-regional phases to the west and southwest, and is close to the REB solution.

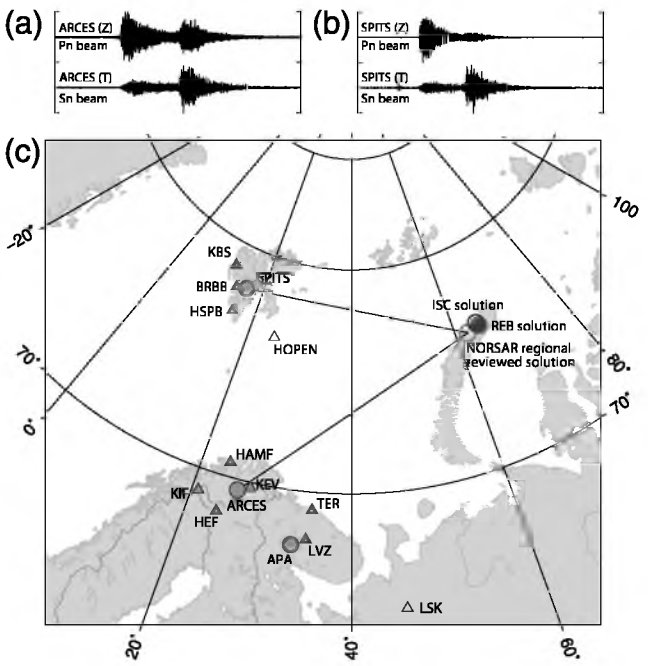

Figure 1. Location estimates for the 11 October 2010 Novaya Zemlya event using regional phases only NORSAR and using global International Monitoring System (IMS) stations (Reviewed Event Bulletin [REB] solution). The International Seismological Center (ISC) location estimate uses both IMS and non-IMS stations, at both regional and teleseismic distances. The stations displayed are those within 15° for which satisfactory readings of both *Pn* and *Sn* phases were made. The regional array stations are labeled with circles and three-component stations with triangles. The waveform segments shown have a duration of 10 min, starting at a time 2010-284:22.48.25. The beams optimized for the *Pn* phases use the vertical channels of the arrays and the beams optimized for the *Sn* phases use the horizontal channels, rotated to be transverse to the great-circle paths indicated by the solid black lines. (see Data and Resources for event-location details).

We seek to provide a more accurate location and origin time for the 11 October event using only data recorded at teleseismic distances. Because the data at far-regional distances comes only from a single direction, it is likely that the solution constrained by purely teleseismic arrivals will be less strongly biased. With a high confidence hypocenter and origin time estimate, derived from teleseismic observations with as broad as possible azimuthal range, we can assess how well different regional velocity models predict the regional arrivals given in Table 1. We seek to modify the best of the 1D models to better predict the regional arrivals observed from this event and evaluate how the location estimates for this event, using only regional phases, vary with the different velocity models. Finally, we consider a low-magnitude event on or close to the northern island of Novaya Zemlya in March 2014. Without ground-truth information or teleseismic observations, we examine the variability of the location estimates possible using the limited observations at regional distances.

Locating the 11 October 2010 Novaya Zemlya Event Using Teleseismic Data

With a magnitude between 4 and 5, the 11 October event is not observed universally at the distances for which teleseismic *P* is anticipated. There is evidence of a signal at many stations for which the phase onset is too poor to be used for the purposes of event location. The seismic network of the International Monitoring System (IMS) for verifying compliance with the Comprehensive Nuclear-Test-Ban Treaty is typically very effective for the detection and location of earthquakes in remote regions given the predominance of array stations. A seismic signal that is right at the background noise level of a single site can be elevated to a clear detection through the stack-and-delay beamforming operation (e.g., Schweitzer, 2014). (The superiority of the IMS seismic arrays over the IMS seismic three-component stations for contributing to built events is demonstrated by Kværna and Ringdal, 2013.) Teleseismic observations from the 11 October event are displayed in Figure 2 and the locations of stations where these signals are recorded are displayed in Figure 3. We specifically tried to focus on the distance range from 23° to 80°,

Table 1
Phase Picks at Regional Distances for the 11 October 2010 Novaya Zemlya Event

Station	Latitude (°)	Longitude (°)	Distance (°)	Azimuth (°)	*Pn* Pick	SNR	*Sn* Pick	SNR
APA	67.603	32.994	12.9	245	22.51.27.95	4.6	22.53.43.01	1.6
ARCES	69.535	25.506	12.6	257	22.51.28.28	28.6	22.53.43.58	4.5
BRBB	78.059	14.219	10.7	303	22.51.02.36	11.2	22.53.00.00	4.0
HAMF	70.642	23.684	12.7	265	22.51.24.92	7.7	22.53.34.26	7.6
HEF	68.406	23.664	14.4	258	22.51.45.12	11.7	22.54.15.33	11.3
HOPEN	76.508	25.011	9.2	291	22.50.39.46	3.0	22.52.14.03	4.6
HSPB	77.002	15.533	10.7	297	22.51.01.50	65.3	22.52.57.90	30.0
KBS	78.926	11.942	10.9	308	22.51.05.17	5.0	22.53.05.34	3.0
KEV	69.755	27.007	12.1	256	22.51.21.90	10.0	22.53.33.42	15.0
KIF	69.043	20.804	14.6	264	22.51.49.31	3.6	22.54.19.66	3.9
LSK	64.879	45.734	13.0	218	22.51.27.35	5.5	22.53.44.56	4.4
LVZ	67.898	34.651	11.9	240	22.51.18.16	4.0	22.53.25.41	8.0
SPITS	78.178	16.370	10.2	303	22.50.56.35	65.0	22.52.49.00	31.2
TER	69.201	35.108	11.1	246	22.51.03.34	10.9	22.52.59.23	6.2

SNR, signal-to-noise ratio.

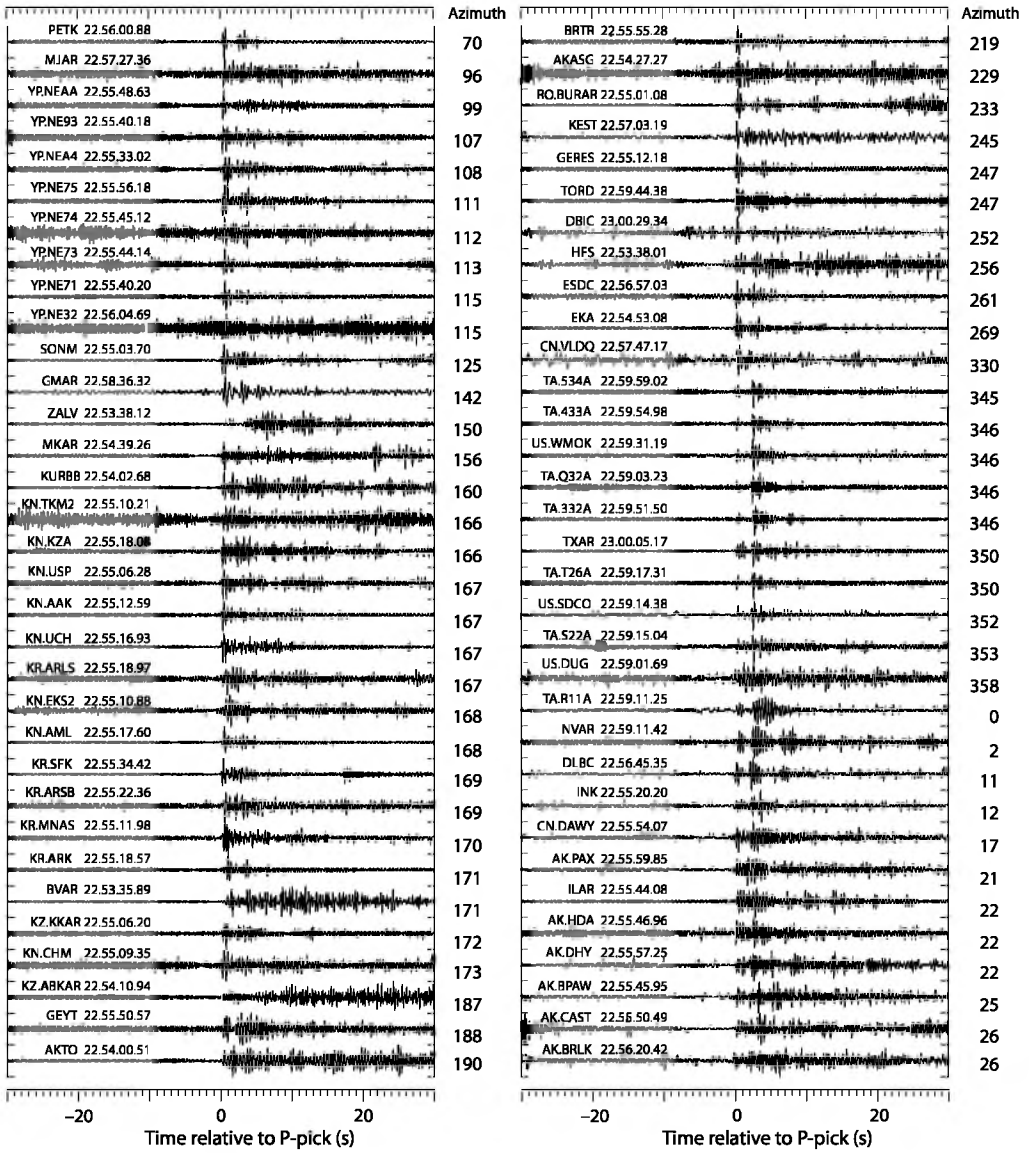

Figure 2. Waveforms from 66 stations at teleseismic distances centered on the *P*-phase arrival. This UT arrival time on 11 October 2010 is given on the trace. Various band-pass filters are applied to optimize the signal-to-noise ratio (SNR). The typical band applied is 1–5 Hz, although this varies somewhat from station to station. For array stations, an optimal beam is displayed. Stations obtained from FDSN networks are preceded by the two character network code. All stations without a network code are IMS stations. The signals are ordered according to station azimuth. The secondary phase (interpreted as a *pP* depth phase) is visible on many traces, arriving approximately 5 s after *P*, although these are clearest on the stations between azimuth 345° and 353°.

avoiding the far-regional distance range in which the global travel times are the least reliable (Myers *et al.*, 2015). This gives a fairly accurate detectability map for the event; although some regions, of course, have very few seismic stations, large regions with few symbols indicate that the event was poorly observed overall. This is the case for almost all of Canada, for example. The most important selection criterion for stations was that the arrival time of the initial *P* phase could be read sufficiently and accurately, although maintaining a reasonably uniform azimuthal distribution was an important consideration. For a region such as Europe, with many satisfactory arrival-time readings on array beams, no attempt was made to find signals on complementary national three-component stations because an excess of stations from one azimuth would likely worsen bias in the solution if not addressed by appropriate weighting. For regions with fewer arrays, all data openly available through the Incorporated Research Institutions for Seismology Data Management Center were obtained in the hope of finding a few stations with low-background noise and/or anomalously high signal-to-noise ratio (SNR). This included temporary deployments of stations such as the Transportable Array (TA) of the US Array project (FDSN network code TA, Levander *et al.*, 1999) and NECESSArray in northeast China (FDSN network code YP, Tao *et al.*, 2014).

Figure 2 displays a trace for each station that is in some way optimal for picking the *P*-wave arrival time. In all cases,

Figure 3. Locations of arrays (circles) and three-component stations (triangles) that recorded teleseismic *P* phases for the 11 October 2010 Novaya Zemlya event with a satisfactory SNR (see Fig. 2). The IMS seismic arrays are labeled. The stations at which the clearest depth phases are shown are displayed with white symbols.

a frequency band was selected, which optimized the SNR, and for the array stations, a stack-and-delay beam was formed, which optimized the alignment of traces in the anticipated direction of arrival. Although only a single filter band (1–5 Hz) is displayed, other bands were considered in making the arrival-time picks. The traces are ordered according to the azimuth from the event location. A small azimuthal band between 345° and 355° contains waveforms which all have a considerably larger amplitude arrival shortly following the initial *P* phase. Most of these stations are temporary sites of the TA, although this arrival is also observed at the TXAR array and a few sites of the United States National Seismic Network. These stations are displayed with white symbols in Figure 3. Were this later arrival to be a depth phase, *pP*—or possibly *sP*, this would provide a significant constraint on the depth of the event and therefore also the origin time. Closer inspection of a few other stations, for example, PETK, CMAR, NVAR, and DLBC, also indicates a second pulse of energy, which could correspond to a depth phase. Figure 4a shows VESPA plots (Davies *et al.*, 1971), which indicate two pulses of coherent energy, separated by approximately 5 s, propagating in a similar direction and recorded at two different seismic arrays at great distance from each other. In Figure 4b, we demonstrate using three of the TA stations that the second phase appears to have a polarity reversal relative to the first phase. The time delay from positive peak to negative peak is between 4.3 and 4.4 s.

Figure 5 shows time residual 1-norm as a function of latitude, longitude, and depth for the *P*-wave arrivals displayed in Figure 2. This is to say that we have placed a trial hypocenter for our event at every point of a 3D grid and solved for the origin time that minimizes the 1-norm of the vector of observed minus predicted travel-time residuals, where the travel time is predicted using the ak135 model of Kennett *et al.* (1995). The white and the blue stars in Figure 5a indicate the REB and NORSAR-reviewed location estimates, respectively (see Data and Resources), and the gray lines indicate the great circle paths to each of the observing stations. The azimuthal coverage is reasonably good and this is reflected in the high degree of azimuthal symmetry in the residual vector norm contours. Figure 5b,c displays the residual norms from this grid-search procedure as a function of depth for the lines CD and AB displayed in the map. The HYPOSAT program allows the depth to be fixed and a best-fit latitude, longitude, and origin time to be found; the small white stars in Figure 5b,c indicate the fixed-depth HYPOSAT solutions and demonstrate that these are consistent with the results of the independent grid-search procedure. We conclude that, using only the initial teleseismic *P*-wave arrivals, the epicenter of the earthquake is at approximately 76.28° N and 64.6° E but with the depth of the event being essentially unconstrained. The trade-off is between the depth and the origin time, the teleseismic *P* arrival times being almost equally consistent with an event at the surface at a time 22:48:26.2, and for example, an event at depth 50 km at time 22:48.32.9. There is not a significant shift in the epicenter as the depth of the hypocenter changes. Bondár *et al.* (2004) demonstrates a good correspondence between the epicenter location accuracy provided by a given teleseismic network and the azimuthal coverage of the recording stations. For the 66 stations at teleseismic distances used for locating the October 2010 event, the secondary azimuthal gap is estimated at about 70° (see Figs. 2 and 5). From studies of GT5 events (i.e., events with epicenter located to within an accuracy of 5 km), Bondár *et al.* (2004) estimated a median mislocation of about 7–9 km for events having a secondary azimuthal gap of less than 70°.

The depth of an event is of great significance for both structural studies, and for example, in the context of screening events from potential violations of a nuclear-test-ban treaty. In the absence of stations in the immediate vicinity of the epicenter, the depth is typically determined by detecting evidence of a surface reflection (e.g., Bonner *et al.*, 2002; Letort *et al.*, 2014, 2015). As with the 1986 Novaya Zemlya/Kara Sea event (Marshall *et al.*, 1989), this event appears to have clear depth phases visible in the waveforms. Ascribing the identification *pP* to each of the observed secondary arrivals and solving using HYPOSAT results in a depth of approximately 13.1 km with an origin time of 22:48:28.2. To assess how sensitive the location is to our identification of these depth phases, a calculation was also performed in which the phases assumed to be *pP* were labeled *sP*. This resulted in a hypocenter with a depth of 9.8 km and an origin time of 22.48.27.6, a very limited change in the source parameters.

The grid-search event-location estimation procedure as displayed in Figure 5 for the ak135 model was also repeated

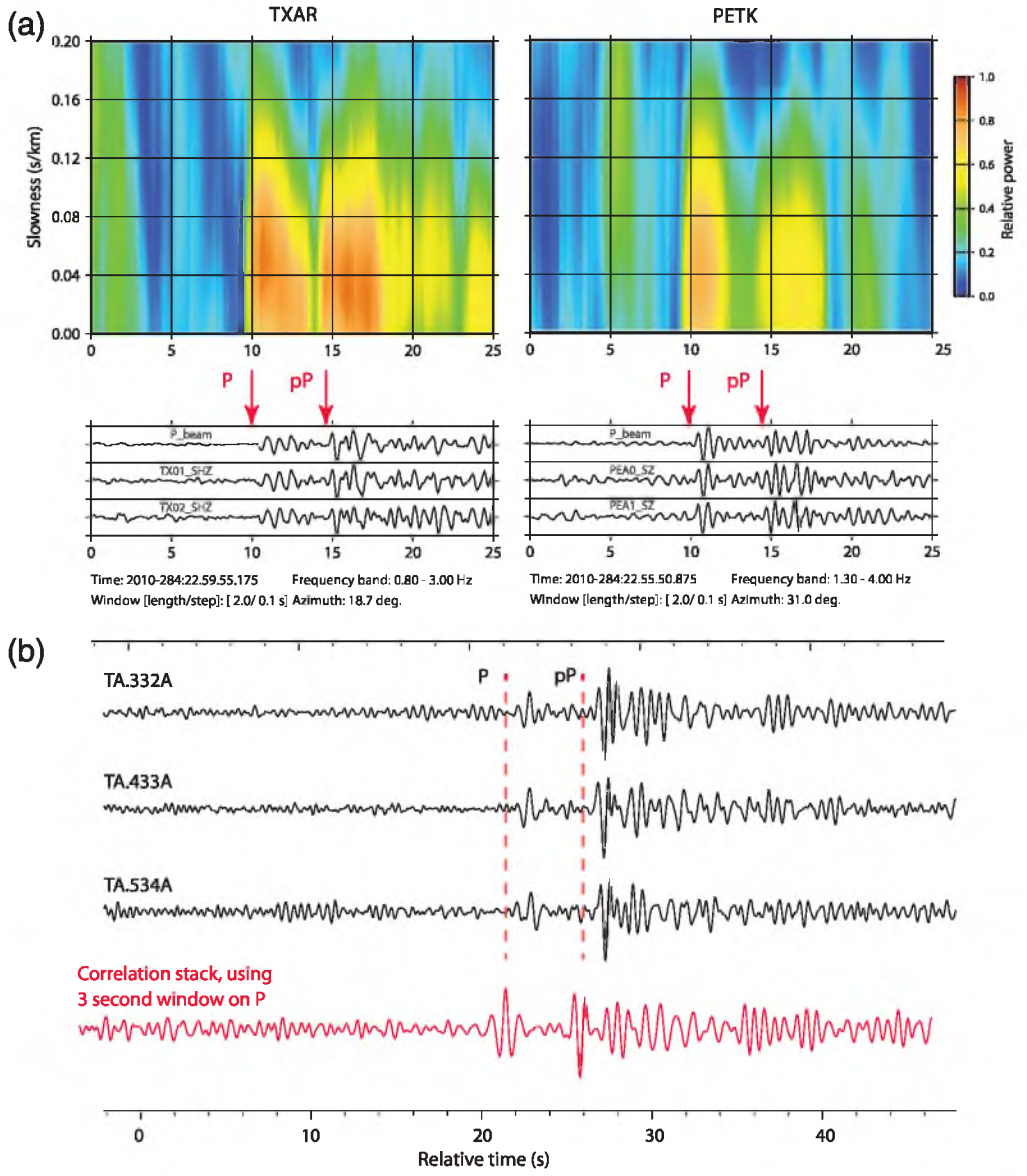

Figure 4. Demonstration of presumed depth phases. (a) The VESPA procedure (Davies *et al.*, 1971) for two seismic arrays and two distinct pulses of energy, separated by approximately 5 s, propagating from the same back azimuth. (b) Waveforms from three stations of the US Array Transportable Array (TA) in the southern United States for which the amplitude of the presumed depth phase is greater than the amplitude for the first *P* arrival. Traces have been aligned according to the arrival picks. The lowermost trace is generated by correlating a tapered multichannel 10-s long template (three channels) with the data stream with the incoming data. A positive peak (the autocorrelation) is followed almost 5 s later by a negative peak.

using travel-time tables constructed using the 3D LLNL-Earth 3D model and LLNL-G3Dv3 raytracing software (Simmons *et al.*, 2012). (A link to the model and software is in Data and Resources.) The hypocenter and origin time that minimized the 1-norm travel-time residual for the 3D model, using both teleseismic *P* and *pP* depth phases, was 76.282° N and 64.692° E, with depth 11.3 km and origin time 22:48:27.8. This solution is within 2 km in depth and within 5 km laterally of the estimate obtained using the 1D ak135 model and the origin time is within 0.4 s. The 1-norm of the travel-time residual vector was 0.405 for the 3D calculation compared with 0.524 for the ak135 calculation, a reduction of approximately 20%.

Evaluating 1D Velocity Models to Explain Regional Arrivals

With a location estimate and origin time based entirely on teleseismic phase picks, we evaluate how well commonly applied velocity models match the observed arrival times for *Pn* and *Sn* at the stations displayed in Figure 1. In addition to the 1D ak135, BAREY and BAREZ models, we consider also *Pn* and *Sn* times predicted using the 3D RSTT models. Figure 6 displays the observed minus predicted travel-time residuals for each of the *Pn* and *Sn* arrival-time picks listed in Table 1 for velocity models as displayed, given an origin

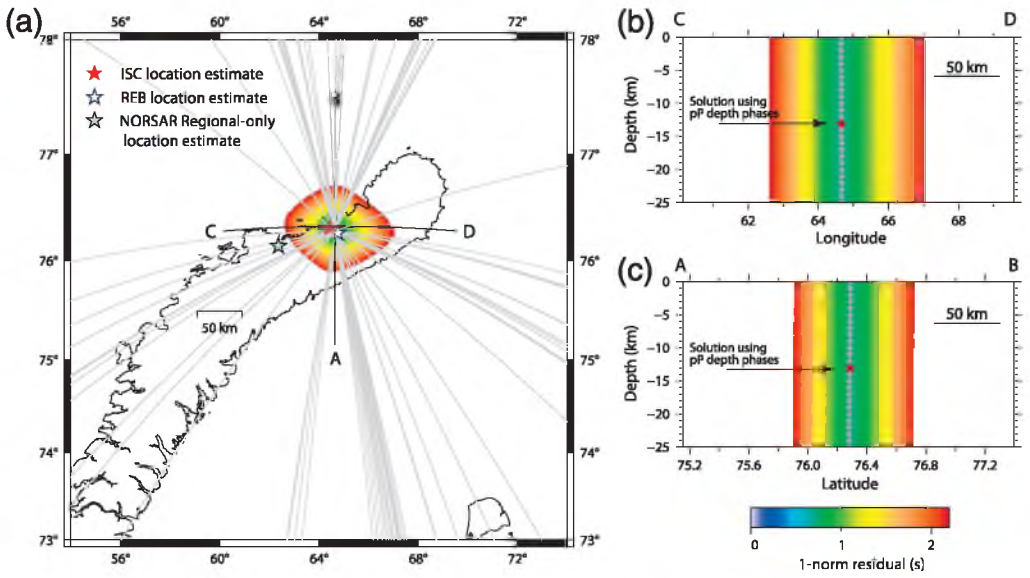

Figure 5. 1-norm residuals for the teleseismic *P* picks displayed in Figure 2 with respect to the ak135 model for trial hypocenters as a function of (a) latitude and longitude with depth fixed to the surface, (b) longitude and depth with latitude fixed to 76.28° N, and (c) latitude and depth with longitude fixed to 64.65° E. For each trial hypocenter, the origin time is selected which minimizes this 1-norm residual. The gray lines show the directions to the stations displayed in Figure 3. The small white stars in panels (b) and (c) indicate HYPOSAT solutions for fixed depth using only teleseismic *P*. The indicated stars in panels (b) and (c) indicate the HYPOSAT solution using *P* and presumed *pP* arrivals without an imposed depth constraint.

time of 2010-284:22.48.28.224, a hypocenter 76.2845° N, 64.6505° E, and depth 13.1 km. The RSTT were calculated both for the software releases in April 2014 (labeled RSTT14) and in October 2010 (labeled RSTT10).

The ak135 model overestimates the *Pn* travel times by up to several seconds for the Barents Sea propagation paths (Fig. 6a). The BAREY and BAREZ models provide as expected a better fit for *Pn* arrivals (the two models having identical *P*-velocity profiles) and the *Pn* predictions from RSTT are very close. RSTT predicts slightly shorter *Pn* travel times for paths from northern Novaya Zemlya to Svalbard than for northern Novaya Zemlya to mainland Fennoscandia. The differences are very small in comparison with the spread in the data, which is likely to be dominated by uncertainty in the arrival-time picks for these largely emergent onsets. The 2014 RSTT *Pn* travel-time estimates from Novaya Zemlya to Svalbard are not significantly different to the estimates from the 2010 RSTT release. For paths from northern Novaya Zemlya to Fennoscandia, the 2014 RSTT release predicts significantly faster travel times than the 2010 RSTT release.

The predictions for *Sn* vary greatly with almost 20 s separating the slowest arrival predictions (ak135) from the fastest (BAREZ) for the stations on mainland Europe (Fig. 6b). The BAREY and BAREZ *S*-velocity models differ only between 41 and 410 km depth with a *P*:*S* velocity ratio of 1.72 for the (faster) BAREZ model and 1.77 for the (slower) BAREY model. The *Sn* phase arrival picks are as expected more spread than the *Pn* picks, although the 7–9 s difference between the BAREY and BAREZ predicted travel times is significantly greater than the 2–3 s variability in the arrival-time estimates. Comparing a linear regression of the BAREZ residual points (3–4 s too fast) and a linear regression of the BAREY residual points (5–7 s too slow) indicates that a modification of BAREY/BAREZ with a *P*:*S* ratio of 1.74 between 41 and 410 km depth would likely fit the observations better. We label this velocity model BS174. The RSTT *Sn* travel-time predictions from the 2010 release are better than the ak135 predictions but significantly poorer than either BAREY or BAREZ. The predictions from the 2014 RSTT release are similar to the BAREY model estimates: far more consistent with the observations than for the 2010 release.

Although the fit for *Pn* is far better than for *Sn*, a 0.5% increase in the upper-mantle *P* velocity can be demonstrated to reduce the absolute residuals in Figure 6a. We call the velocity model with the *S*-wave velocity structure of BS174, combined with this marginally increased *P*-wave velocity profile NZ2010. The *P*- and *S*-velocity profiles for BAREY and BAREZ, together with the modifications, are displayed in Figure 7 and tabulated in Table 2.

Travel-time residuals as displayed in Figure 6 were calculated for a large number of alternative candidate hypocenters and origins, which were similarly consistent with the teleseismic observations. Although small perturbations to the latitude, longitude, depth, and time of the source resulted in small changes to the travel-time residuals, the patterns displayed in Figure 6 appear to hold for all likely source locations and origin times.

Although we can draw conclusions as to the suitability of velocity models by examining the residuals as displayed in Figure 6, the true test is the influence the models have on event location. If we attempt to locate the 11 October event ignoring all stations at distances greater than 15°, we are left

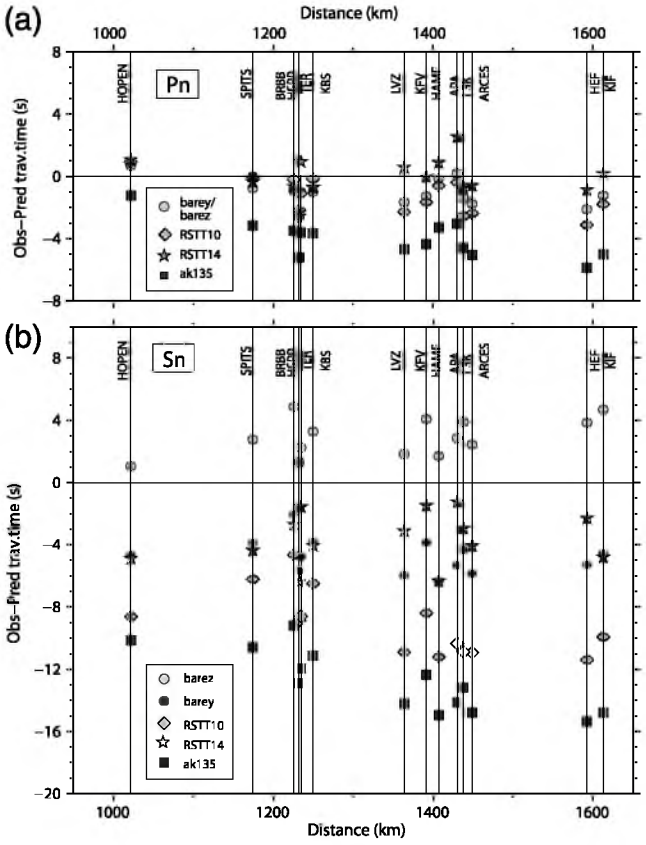

Figure 6. Time residuals with respect to the arrival-time picks given in Table 1 using different models using an event origin time of 2010-284:22.48.28.224 and a hypocenter 76.2845° N, 64.6505° E, and depth 13.1 km. The travel times computed for the 1D models ak135, BAREY, and BAREZ are not dependent upon the direction, whereas those for the Regional Seismic Travel Time (RSTT) model are calculated point to point using the RSTT software.

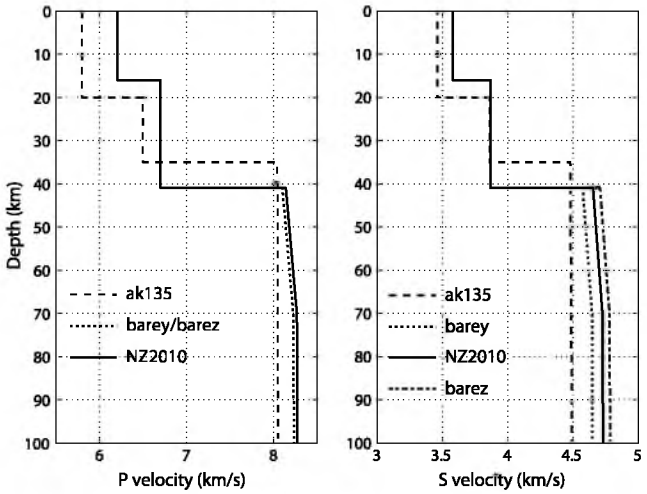

Figure 7. Velocity as a function of depth for the ak135, BAREY, and BAREZ models together with NZ2010: the modification to BAREY/BAREZ, which appears to give the best fit to the regional arrival times listed in Table 1 for the purely teleseismic hypocenter and origin time for the 11 October 2010 event.

with the arrival-time readings provided in Table 1. Figure 8 displays location estimates using only these phase arrivals and the velocity models as indicated together with the teleseismic reference location. That the NZ2010 model location comes closest to the reference location is not in itself significant; the modifications to the velocity profiles were chosen specifically to optimize the fit for exactly these arrivals. What is of greatest interest is the geographical bias resulting from applying different velocity models when the observing stations all lie within an azimuth band of width 90° from the event's true location. The faster *S*-wave velocities in the BAREZ model pull the preferred location almost 50 km to the east. The slower BAREY model *S* velocities draw the event a similar distance to the west. In the absence of stations in the wide azimuthal gap, it is the *S*-wave arrivals that primarily constrain the distance the event appears to be from the observing stations to the west and southwest. Figure 8 gives an impression of the extent to which the event locations are subject to uncertainty in the *S*-wave velocity models. The spread in the event-location estimate for regional stations and different velocity models is over an order of magnitude greater than the anticipated uncertainty in the event location from the teleseismic observations. A similar observation was made by Schweitzer and Kennett (2007).

Consequences for Regional Event Location

On 4 March 2014, a far smaller event occurred on or close to the northern island of Novaya Zemlya. With an approximate magnitude of 3, this event is far more typical of the Novaya Zemlya seismicity that needs to be detected, located, and classified. Signals from this event were only recorded well on a very limited number of stations. The signal on the SPITS array is by far the best observed, although the recordings on ARCES and KBS are sufficient for *Pn* and *Sn* arrival times to be read with a sufficient accuracy for use in location procedures. Although there are now far more stations than previously in northern Fennoscandia and on Svalbard, the SNR for an event of this magnitude is still too low on most stations for these recordings to be useful. The monitoring at low magnitudes for the region is still dominated by the SPITS and ARCES arrays and only the very best of the network three-component stations. This event is interesting from a location perspective because it is also observed on the new station ZFI2 on Franz Josef Land (see Morozov *et al.*, 2015). Figure 9 displays traces optimized for the observation of *Pn* and *Sn* at the ZFI2, SPITS, ARCES, and KBS stations. Signals on all other available stations were deemed to be of too poor quality for use in the location procedure.

The March 2014 event is about 300 km further south than the 11 October 2010 event, and depending upon the significance of the 3D velocity structure, the performance of the 1D models may be significantly different to that observed for the northern tip of Novaya Zemlya. It is important to note that, for this event, we have no ground truth and no independent seismic observations that can constrain the event location. The *Pn* and

Table 2
Specification of *P*- and *S*-Wave Velocities for Travel-Time Prediction in the Barents Sea Region

Depth (km)	$V_P^{A,B,C}$	V_P^D	V_S^A	$V_S^{C,D}$	V_S^B
0.0	6.200	6.200	3.580	3.580	3.580
16.0	6.200	6.200	3.580	3.580	3.580
16.0	6.700	6.700	3.870	3.870	3.870
41.0	6.700	6.700	3.870	3.870	3.870
41.0	8.100	8.141	4.576	4.655	4.709
70.0	8.225	8.266	4.647	4.727	4.782
210.0	8.260	8.301	4.667	4.747	4.802
210.0	8.350	8.392	4.718	4.799	4.810
410.0	9.030	9.030	4.870	4.870	4.870
410.0	9.360	9.360	5.080	5.080	5.080
460.0	9.528	9.528	5.186	5.186	5.186

From a depth of 410 km and greater, all models are identical to ak135 (Kennett *et al.*, 1995). All velocities are specified in kilometers per seconds and the superscripts identify the appropriate velocity models: BAREY (A), BAREZ (B), BS174 (C), and NZ2010 (D).

Sn phase arrival times listed in Table 3 are the only pieces of information we have to locate the event. For each of the models ak135, BAREY, NZ2010, and BAREZ, we locate the event using HYPOSAT (depth fixed to the surface) using two different networks. We consider the network comprising ARCES, SPITS, and KBS, which has recorded most of the low-magnitude Novaya Zemlya events over the previous two decades, and then the full set of stations displayed in Figures 9 and 10a.

Figure 10b shows the location estimates for the 3- and 4-station configurations using the models as indicated. The ak135 model places the event at sea. The BAREY and BAREZ models place the event at the west and east coasts of the northern island of Novaya Zemlya, respectively. The NZ2010 model with its intermediate upper-mantle *S*-velocity structure places the event on land approximately halfway between the east and west coasts. Numerous attempts were made to locate the events using arrival-time estimates perturbed slightly from the times provided in Table 3 and this was found to have a negligible result in the location estimates; the *S*-wave velocity model is far more significant. The time-residual norms for the ak135 model are significantly higher than for the other models, although the minimum time residual alone is not sufficient to favor any one of the BAREY, NZ2010, or BAREZ models over any of the others. If a 1D velocity model provides reasonable fidelity over the region to which it is supposed to apply, then the location estimate made using the 4-station network should not differ greatly from that made using the 3-station network. Although the differences are not large, the solutions using the NZ2010 model are moved less by the addition of the readings from the ZFI2 station than the solutions resulting from the BAREY or BAREZ models.

A grid-search location estimate for the 4 March event using travel times calculated from the 2014 release of RSTT results in inland location estimates essentially collocated with the location estimates obtained using the BAREY 1D model.

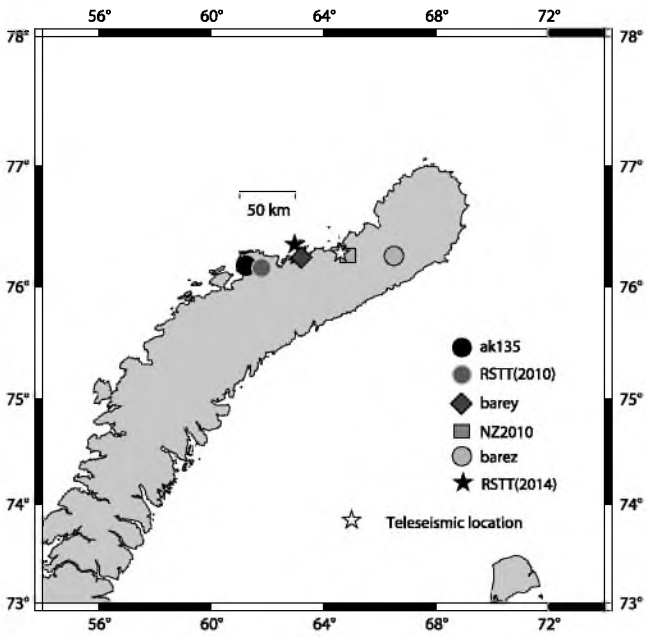

Figure 8. Location estimates for the 11 October 2010 Novaya Zemlya event using regional data only (14 stations, *Pn* and *Sn* readings listed in Table 1), together with the reference teleseismic location estimate.

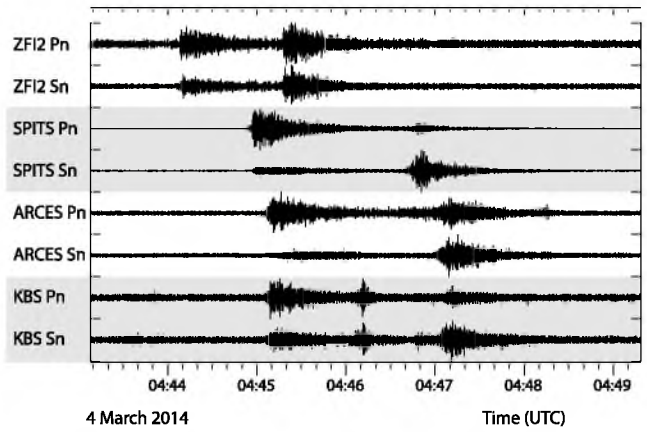

Figure 9. Regional waveforms for stations as indicated for the 4 March 2014 Novaya Zemlya event. All *Pn* traces are vertical components only with the ARCES beam formed using $V_{app} = 9.1$ km/s and back azimuth 54° and the SPITS beam formed using $V_{app} = 7.4$ km/s and back azimuth 107°. All *Sn* traces are constructed from transverse rotations of horizontal components with the ARCES beam formed using $V_{app} = 5.1$ km/s and back azimuth 54° and the SPITS beam formed using $V_{app} = 4.7$ km/s and back azimuth 107°. All beams are band-pass filtered 4–10 Hz.

Conclusions

The ability to locate low-magnitude seismic events in the European Arctic requires excellent models for seismic-wave velocities in the crust and upper mantle. This is primarily because we are only able to monitor from the northernmost part of mainland Europe and from Svalbard. The m_b 4.5 earthquake close to the northern tip of Novaya Zemlya on

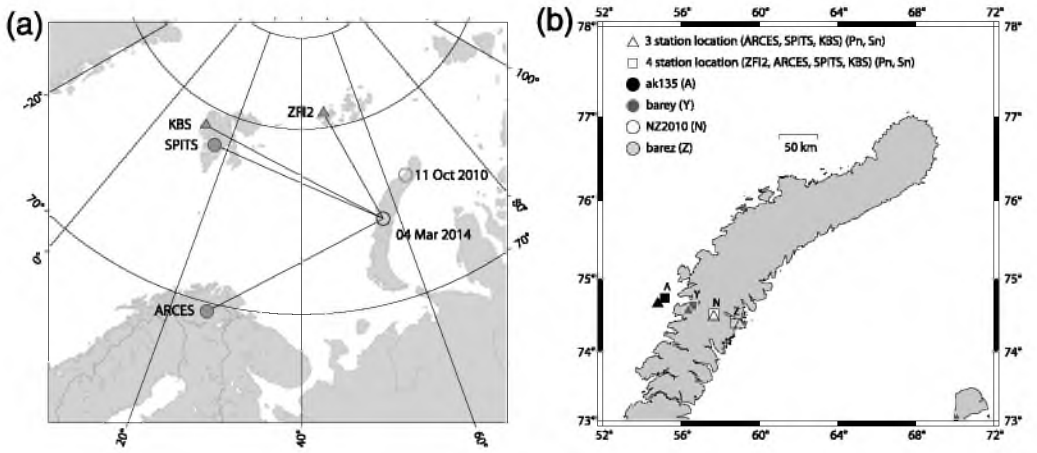

Figure 10. (a) Regional stations recording the 4 March 2014 Novaya Zemlya event and (b) event-location estimates of the event using different velocity models. The location estimates obtained using the 2014 release of RSTT are almost identical to those obtained using the BAREY model.

11 October 2010 is unique among seismic events in this part of the world as it is, to date, the only event that has been recorded both on the regional seismic networks of the European Arctic and globally at teleseismic distances. By careful consideration of teleseismic signals, we estimate the epicenter to be 76.28° N, 64.65° E with a likely uncertainty of only a few kilometers. Clear depth phases are observed on many stations, but are strongest on stations in the southern United States. Assuming these phases to be *pP* provides a depth estimate of approximately 12 km and a corresponding origin time of 2010-284:22.48.28.2.

Given that this teleseismic location estimate is entirely independent of the many observations at distances of 20° or less, we can use this hypocenter and origin time estimate to evaluate velocity models for predicting regional travel times. We evaluated a number of commonly applied 1D velocity models in addition to the 3D RSTT software. The BAREY/BAREZ and RSTT models predict the *Pn* arrivals at stations within 15° of the epicenter relatively well, although it appears that the travel times are slightly overestimated particularly for the paths toward mainland Europe. There is, however, a very large spread in the time residuals for the *Sn* phases. Most of the models predict *Sn* arrivals that are significantly too late, with the exception of the BAREZ model that slightly underestimates the travel time. The BAREY and BAREZ models differ only by the *P*:*S* velocity ratio in the upper mantle (1.72 for BAREY and 1.77 for BAREZ) and a new 1D model BS174 (identical to BAREY/BAREZ except for a 1.74 *P*:*S* velocity ratio) reduces the *Sn* residuals significantly. A second model NZ2010 with the same *S*-velocity profile as BS174 but with a 0.5% increase in *P* velocities between 41 and 410 km depth in addition minimizes the *Pn* time residuals. We hope also that the data presented here will be of use in subsequent 3D tomographic studies. The scarcity of well-observed events in this region makes the body-wave arrival data of great interest.

The increase in the number of stations in the European Arctic in recent years has been of great benefit in providing many regional observations of the 11 October 2010 earthquake. The modifications made to the BAREY/BAREZ velocity models were made on the basis of observing the residuals displayed in Figure 6. If we had only three or four stations with satisfactory regional phases, the confidence in the significance of the time residuals would have been substantially lower. However, as the March 2014 event demonstrated, the detection capability for events in the European Arctic at the lowest magnitudes is still controlled by the SPITS and ARCES seismic arrays and the most sensitive of the closest three-component stations. (Newly deployed instruments such as the ZFI2 station may have significance in future years.) We have reason to believe that the *Pn* travel times predicted by the 1D BAREY/BAREZ models, and also by the 3D RSTT model, perform well for events in this region. The failing of the existing models appears to be in the *Sn* travel-time predictions that appear to be the most significant factor in the location estimate uncertainties. The 2010 release of RSTT appears to overestimate the *Sn* travel times from this region of the European Arctic significantly. The 2014 RSTT release predicts *Sn* travel times that are comparable to those predicted by the BAREY model, providing an improvement on the 2010 release but still based on velocity estimates that are slightly too low. Together with local 1D models based on, for example, receiver function studies (e.g., Morozov *et al.*, 2015), we hope that the data presented in this article will contribute to a significant improvement in the coming iterations of the 3D models for the crust and uppermost mantle.

The teleseismic depth phases were significant for providing an independent constraint on the event depth, and consequently, the origin time. It is important to note that although there was evidence at many stations for depth phases, they were clearest at a very small number of stations with most of the best recordings being on temporary deployments. We would advocate paying greater attention to depth phases, both in applying advanced techniques for

Table 3
Phase Picks for the 4 March 2014, Novaya Zemlya Event

Station	Latitude (°)	Longitude (°)	Distance (°)	Azimuth (°)	*Pn* Pick	SNR	*Sn* Pick	SNR
ARCES	69.535	25.506	11.0	260	04.45.06.08	2.2	04.47.02.17	5.0
KBS	78.926	11.942	11.0	314	04.45.06.36	1.6	04.47.04.26	4.1
SPITS	78.178	16.370	10.2	310	04.44.55.53	7.5	04.46.42.98	4.6
ZFI2	80.809	47.655	6.7	346	04.44.08.32	3.9	04.45.17.20	3.5

their detection (e.g., Letort *et al.*, 2015), and in searching additional waveforms. Events that are well constrained in time and space using teleseismic data may have a greater role than previously assumed in the calibration of regional velocity models in the absence of ground-truth explosion sources. We also demonstrated that cross-border collaboration in the sharing and analysis of seismic data has significant benefits in optimizing the exploitation of the available observations.

Data and Resources

Waveform data from the SPITS and ARCES arrays are available openly from http://www.norsardata.no/NDC/data/autodrm.html (last accessed March 2016). The APA, TER, and BRBB stations are operated by the Kola Regional Seismological Center (KRSC) in Apatity, Russia, and the LSK station is operated by the Institute of Environmental Problems of the North of the Ural Branch of the Russian Academy of Sciences, in Arkhangelsk, Russia. The HSPB station is operated by the Institute of Geophysics of the Polish Academy of Sciences, Warzawa, Poland. The stations HOPEN and HAMF are operated by the University of Bergen, Norway, and are part of the Norwegian National Seismic Network (NNSN). The stations HEF and KIF are part of the Finnish National Seismic Network and operated by the University of Helsinki (data available from geofon.gfz-potsdam.de/waveform/, last accessed March 2016). Data from the stations KEV, KBS, and LVZ are obtained from the Incorporated Research Institutions for Seismology (IRIS) Data Management Center (DMC) at http://ds.iris.edu/SeismiQuery/by_station.html (last accessed March 2016) from the IU and II networks. Waveform data from International Monitoring System (IMS) stations were obtained from the International Data Center (IDC) in Vienna, Austria. Waveform data from the Canadian National Seismograph Network (CNSN) were obtained from Natural Resources Canada at http://www.earthquakescanada.nrcan.gc.ca/stndon/AutoDRM/autodrm_req-eng.php (last accessed March 2016). All additional waveforms were obtained via the IRIS-DMC. We utilized data from the networks AK, KN, KR, KZ, RO, TA, and YP and gratefully acknowledge the operators of these networks for making the data available. The event locations displayed are taken from the NORSAR Reviewed Regional Event Bulletin available at http://www.norsardata.no/NDC/bulletins/regional/ (last accessed March 2016). The reviewed location of the 11 October 2010 event is found on http://www.norsardata.no/NDC/bulletins/regional/2010/10/14009.html (last accessed March 2016). The LLNL-G3D global 3D *P*-wave velocity model and raytracing software is available from https://missions.llnl.gov/nonproliferation/nuclear-explosion-monitoring/global-3d-seismic-tomography (last accessed March 2016). The Regional Seismic Travel Time (RSTT) software is available openly from http://www.sandia.gov/rstt/ (last accessed March 2016). The seismic bulletin of the International Seismological Center is available from http://www.isc.ac.uk/ (last accessed March 2016).

Acknowledgments

This effort was partly funded by the NORRUSS Project "Seismological monitoring of geophysical processes in the European Arctic," Research Council of Norway Project Number 233973/H30, and Russian Fund of Basic Research Grant Number 14-05-93080. We are grateful to Nathan Simmons and an anonymous reviewer for insightful comments and recommendations. All maps in this article are created using Generic Mapping Tool (GMT) software (Wessel and Smith, 1995). We are grateful to Ulf Baadshaug at NORSAR for technical assistance.

References

Baumgardt, D. R. (2001). Sedimentary basins and the blockage of *Lg* wave propagation in the continents, *Pure Appl. Geophys.* **158,** no. 7, 1207–1250, doi: 10.1007/PL00001221.

Bondár, I., S. C. Myers, E. R. Engdahl, and E. A. Bergman (2004). Epicentre accuracy based on seismic network criteria, *Geophys. J. Int.* **156,** no. 3, 483–496, doi: 10.1111/j.1365-246x.2004.02070.x.

Bonner, J. L., D. T. Reiter, and R. H. Shumway (2002). Application of a cepstral f statistic for improved depth estimation, *Bull. Seismol. Soc. Am.* **92,** no. 5, 1675–1693, doi: 10.1785/0120010128.

Bungum, H., O. Ritzmann, N. Maercklin, J. I. Faleide, W. D. Mooney, and S. T. Detweiler (2005). Three-dimensional model for the crust and upper mantle in the Barents Sea region, *Eos Trans. AGU* **86,** no. 16, 160–161, doi: 10.1029/2005EO160003.

Davies, D., D. J. Kelly, and J. R. Filson (1971). The VESPA process for the analysis of seismic signals, *Nature* **232,** 8–13.

Gibbons, S. J., J. Schweitzer, F. Ringdal, T. Kværna, S. Mykkeltveit, and B. Paulsen (2011). Improvements to seismic monitoring of the European Arctic using three-component array processing at SPITS, *Bull. Seismol. Soc. Am.* **101,** no. 6, 2737–2754, doi: 10.1785/0120110109.

Hauser, J., K. M. Dyer, M. E. Pasyanos, H. Bungum, J. I. Faleide, S. A. Clark, and J. Schweitzer (2011). A probabilistic seismic model for the European Arctic, *J. Geophys. Res.* **116,** no. B1, doi: 10.1029/2010jb007889.

Hicks, E. C., T. Kværna, S. Mykkeltveit, J. Schweitzer, and F. Ringdal (2004). Travel-times and attenuation relations for regional phases in the Barents Sea region, *Pure Appl. Geophys.* **161,** 1–19.

Kennett, B. L. N., and E. R. Engdahl (1991). Traveltimes for global earthquake location and phase identification, *Geophys. J. Int.* **105,** no. 2, 429–465, doi: 10.1111/j.1365-246x.1991.tb06724.x.

Kennett, B. L. N., E. R. Engdahl, and R. Buland (1995). Constraints on seismic velocities in the Earth from travel times, *Geophys. J. Int.* **122,** 108–124.

Khalturin, V. I., T. G. Rautian, P. G. Richards, and W. S. Leith (2005). A review of nuclear testing by the Soviet Union at Novaya Zemlya, 1955–1990, *Sci. Global Secur.* **13,** nos. 1/2, 1–42, doi: 10.1080/08929880590961862.

Kremenetskaya, E., V. Asming, and F. Ringdal (2001). Seismic location calibration of the European Arctic, *Pure Appl. Geophys.* **158,** no. 1, 117–128, doi: 10.1007/pl00001151.

Kværna, T., and F. Ringdal (2013). Detection capability of the seismic network of the International Monitoring System for the Comprehensive Nuclear-Test-Ban Treaty, *Bull. Seismol. Soc. Am.* **103,** no. 2A, 759–772, doi: 10.1785/0120120248.

Letort, J., J. Guilbert, F. Cotton, I. Bondár, Y. Cano, and J. Vergoz (2015). A new, improved and fully automatic method for teleseismic depth estimation of moderate earthquakes (4.5 < mag < 5.5): Apphcation to the Guerrero subduction zone (Mexico), *Geophys. J. Int.* **201,** no. 3, 1834–1848, doi: 10.1093/gji/ggv093.

Letort, J., J. Vergoz, J. Guilbert, F. Cotton, O. Sebe, and Y. Cano (2014). Moderate earthquake teleseismic depth estimations: New methods and use of the Comprehensive Nuclear-Test-Ban Treaty Organization network data, *Bull. Seismol. Soc. Am.* **104,** no. 2, 593–607, doi: 10.1785/0120130126.

Levander, A., E. D. Humphreys, G. Ekstrom, A. S. Meltzer, and P. M. Shearer (1999). Proposed project would give unprecedented look under North America, *Eos Trans. AGU* **80,** no. 22, 245–251, doi: 10.1029/99eo00181.

Levshin, A., and K. A. Berteussen (1979). Anomalous propagation of surface waves in the Barents Sea as inferred from NORSAR recordings, *Geophys. J. Int.* **56,** no. 1, 97–118, doi: 10.1111/j.1365-246x.1979.tb04770.x.

Levshin, A. L., J. Schweitzer, C. Weidle, N. M. Shapiro, and M. H. Ritzwoller (2007). Surface wave tomography of the Barents Sea and surrounding regions, *Geophys. J. Int.* **170,** no. 1, 441–459, doi: 10.1111/j.1365-246x.2006.03285.x.

Marshall, P. D., R. C. Stewart, and R. C. Lilwall (1989). The seismic disturbance on 1986 August 1 near Novaya Zemlya: A source of concern? *Geophys. J. Int.* **98,** no. 3, 565–573, doi: 10.1111/j.1365-246X.1989.tb02290.x.

McCowan, D. W., P. Glover, and S. S. Alexander (1978). A crust and upper mantle model for Novaya Zemlya from Rayleigh-wave dispersion data, *Bull. Seismol. Soc. Am.* **68,** no. 6, 1651–1662.

Morozov, A. N., and Y. V. Konechnaya (2013). Monitoring of the Arctic region: Contribution of the Arkhangelsk seismic network, *J. Seismol.* **17,** no. 2, 819–827, doi: 10.1007/s10950-012-9356-x.

Morozov, A. N., N. V. Vaganova, Y. V. Konechnaya, and V. E. Asming (2015). New data about seismicity and crustal velocity structure of the "continent-ocean" transition zone of the Barents–Kara region in the Arctic, *J. Seismol.* **19,** no. 1, 219–230, doi: 10.1007/s10950-014-9462-z.

Murphy, J. R., W. Rodi, M. Johnson, D. D. Sultanov, T. J. Bennett, M. N. Toksöz, V. Ovtchinnikov, B. W. Barker, D. T. Reiter, A. C. Rosca, *et al.* (2005). Cahbration of International Monitoring System (IMS) stations in central and eastern Asia for improved seismic event location, *Bull. Seismol. Soc. Am.* **95,** no. 4, 1535–1560, doi: 10.1785/0120040087.

Myers, S. C., M. L. Begnaud, S. Ballard, M. E. Pasyanos, W. S. Phillips, A. L. Ramirez, M. S. Antohk, K. D. Hutchenson, J. J. Dwyer, C. A. Rowe, *et al.* (2010). A crust and upper-mantle model of Eurasia and North Africa for Pn travel-time calculation, *Bull. Seismol. Soc. Am.* **100,** no. 2, 640–656, doi: 10.1785/0120090198.

Myers, S. C., N. A. Simmons, G. Johannesson, and E. Matzel (2015). Improved regional and teleseismic *P*-wave travel-time prediction and event location using a global 3D velocity model, *Bull. Seismol. Soc. Am.* **105,** no. 3, 1642–1660, doi: 10.1785/0120140272.

Phillips, W. S., M. L. Begnaud, C. A. Rowe, L. K. Steck, S. C. Myers, M. E. Pasyanos, and S. Ballard (2007). Accounting for lateral variations of the upper mantle gradient in *Pn* tomography studies, *Geophys. Res. Lett.* **34,** no. 14, doi: 10.1029/2007gl029338.

Ringdal, F. (1997). Study of low-magnitude seismic events near the Novaya Zemlya test site, *Bull. Seismol. Soc. Am.* **87,** 1563–1575.

Ritzmann, O., and J. I. Faleide (2009). The crust and mantle hthosphere in the Barents Sea/Kara Sea region, *Tectonophysics* **470,** nos. 1/2, 89–104, doi: 10.1016/j.tecto.2008.06.018.

Ritzmann, O., N. Maercklin, J. I. Faleide, H. Bungum, W. D. Mooney, and S. T. Detweiler (2007). A three-dimensional geophysical model of the crust in the Barents Sea region: Model construction and basement characterization, *Geophys. J. Int.* **170,** no. 1, 417–435, doi: 10.1111/j.1365-246x.2007.03337.x.

Schweitzer, J. (2001). HYPOSAT—An enhanced routine to locate seismic events, *Pure Appl. Geophys.* **158,** no. 1, 277–289, doi: 10.1007/pl00001160.

Schweitzer, J. (2014). Seismometer arrays, in *Encyclopedia of Earthquake Engineering*, M. Beer, I. A. Kougioumtzoglou, E. Patelh, and I. S. Au (Editors), Springer, Berlin/Heidelberg, 1–11, doi: 10.1007/978-3-642-36197-5_191-1.

Schweitzer, J., and B. L. N. Kennett (2007). Comparison of location procedures: The Kara Sea event of 16 August 1997, *Bull. Seismol. Soc. Am.* **97,** no. 2, 389–400, doi: 10.1785/0120040017.

Simmons, N. A., S. C. Myers, G. Johannesson, and E. Matzel (2012). LLNL-G3Dv3: Global *P* wave tomography model for improved regional and teleseismic travel time prediction, *J. Geophys. Res.* **117,** no. B10, doi: 10.1029/2012jb009525.

Simmons, N. A., S. C. Myers, G. Johannesson, E. Matzel, and S. P. Grand (2015). Evidence for long-hved subduction of an ancient tectonic plate beneath the southern Indian Ocean, *Geophys. Res. Lett.* **42,** no. 21, doi: 10.1002/2015gl066237.

Tao, K., F. Niu, J. Ning, Y. J. Chen, S. Grand, H. Kawakatsu, S. Tanaka, M. Obayashi, and J. Ni (2014). Crustal structure beneath NE China imaged by NECESSArray receiver function data, *Earth Planet. Sci. Lett.* **398,** 48–57, doi: 10.1016/j.epsl.2014.04.043.

Wessel, P., and W. H. F. Smith (1995). New version of the Generic Mapping Tools, *Eos Trans. AGU* **76,** 329.

Yang, X., I. Bondár, K. McLaughhn, and R. North (2001). Source specific station corrections for regional phases at Fennoscandian stations, *Pure Appl. Geophys.* **158,** no. 1, 35–57, doi: 10.1007/pl00001164.

NORSAR
P.O. Box 53
2027 Kjeller, Norway
steven.gibbons@norsar.no
(S.J.G., T.K., J.S.)

Federal Center for Integrated Arctic Research
The Russian Academy of Sciences
Severnoj Dviny Emb., 23
Arkhangelsk 163000, Russia
(G.A., Y.V.K., N.V.V.)

Kola Branch of the Geophysical Survey of the Russian Academy of Sciences
Fersmana Street, 14
184209 Apatity
Murmansk Region, Russia
(V.A., E.K.)

Manuscript received 26 April 2016;
Published Online 14 June 2016